bioRxiv preprint doi: https://doi.org/10.1101/2024.03.20.585966; this version posted March 23, 2024. The copyright holder for this preprint (which was not certified by peer review) is the author/funder. All rights reserved. No reuse allowed without permission.

Screening of glucose binding proteins for the development of biosensors

Anurag Makare[a#], Amit Chaudhary[a#], Debankita De[b], Parijat Deshpande[b], Ajay Singh Panwar[a]*

[a]Department of Metallurgical Engineering & Materials Science, Indian Institute of Technology Bombay, India 400076

[b]Tata Research Development and Design Centre Pune, Maharashtra, India, 411013

***Corresponding author**
Department of Metallurgical Engineering & Materials Science
Indian Institute of Technology Bombay, India 400076
panwar@iitb.ac.in

bioRxiv preprint doi: https://doi.org/10.1101/2024.03.20.585966; this version posted March 23, 2024. The copyright holder for this preprint (which was not certified by peer review) is the author/funder. All rights reserved. No reuse allowed without permission.

ABSTRACT

Selecting suitable glucose binding proteins (GBPs) is vital for biosensor development for medical diagnostics and quality control in food industry. Biosensors offer advantages such as high specificity, selectivity, fast response time, continuous measurement, and cost-effectiveness. The current work utilized a combination of molecular docking, molecular dynamics (MD) simulations and free energy calculations to develop a high-throughput bioinformatics pipeline to select GBP candidates from an extensive protein database. GBPs with good binding affinity to glucose were virtually screened from Protein Data Bank using molecular docking. MD simulations ascertained the binding dynamics of a few selected candidates. Further, steered MD (Brownian dynamics fluctuation-dissipation-theorem) was used to estimate binding free energies of the ligand-protein complex. Correlations between ligand-binding parameters obtained from relatively longer MD simulations and binding parameters interpreted from faster docking simulations were investigated. The correlation plots suggested that, a combination of threshold values of the following three docking parameters; docking binding energy, binding cavity depth and the number of hydrogen bonds between the ligand and binding site residues can be used to reliably predict candidate GBPs. Thus, a high-throughput and accurate protein selection process based on relatively faster docking simulations was proposed to screen GBPs for glucose biosensing.

KEYWORDS: Glucose binding proteins, glucose sensing, high-throughput screening, molecular dynamics simulation

bioRxiv preprint doi: https://doi.org/10.1101/2024.03.20.585966; this version posted March 23, 2024. The copyright holder for this preprint (which was not certified by peer review) is the author/funder. All rights reserved. No reuse allowed without permission.

1. Introduction

Biosensors have revolutionized a wide range of fields, from medical diagnostics to environmental monitoring, by combining the specificity of biomolecular recognition with the sensitivity of modern sensing technologies(Singh et al., 2020). These powerful devices enable real-time and accurate detection of analytes in complex biological or environmental samples. Proteins are versatile candidates for recognition elements in biosensors, offering unique binding capabilities and adaptability(Bag & Mandal, 2023; Butt et al., 2023; Chadha et al., 2022; Pullano et al., 2022). Glucose biosensing is crucial in medical diagnostics and blood glucose monitoring. In numerous applications, such as diabetes management, food industry quality control, and fermentation processes, the precise measurement of glucose is of paramount importance due to its role as an essential energy source(Pullano et al., 2022; Yoo & Lee, 2010). Glucose biosensors employ specific enzymes for accurate glucose measurement. Continuous Glucose Monitoring Systems provide real-time data wirelessly to monitors or smartphones (Bankar et al., 2009; Guilbault & Lubrano, 1973; Weibel & Bright, 1971). Non-invasive glucose biosensors offer less invasive monitoring through optical and electrochemical methods. These advancements enhance diabetes management, promising ongoing improvements in accuracy and convenience(Klonoff, 1997; Larin et al., 2002; MacKenzie et al., 1999; Rabinovitch et al., 1982; Rassel et al., 2020; Richiardi et al., 2013).

To achieve high selectivity and sensitivity in glucose sensing, the selection of an appropriate recognition element becomes critical. In this context, glucose binding proteins (GBPs) are promising candidates owing to their innate ability to selectively bind glucose molecules. GBPs encompass a diverse group of proteins with distinct binding pockets or domains that exhibit an affinity for glucose. As recognition elements in biosensors, GBPs offer advantages of high binding affinity, specificity and stability. Moreover, their potential for genetic and protein engineering allows for performance enhancement and customization to specific applications. The screening and selection of suitable GBPs for biosensor development constitute crucial steps in harnessing their potential. To this end, advanced screening techniques, including combinatorial libraries, phage display, and high-throughput screening methods(Kaczmarek & Prather, 2021; Yeom et al., 2018; Zhang & Qian, 2023), have facilitated the identification of novel GBPs with enhanced binding properties. These techniques enable the exploration of vast protein libraries and the identification of GBPs with desired attributes, such as high affinity, selectivity, and resistance to interfering substances.

bioRxiv preprint doi: https://doi.org/10.1101/2024.03.20.585966; this version posted March 23, 2024. The copyright holder for this preprint (which was not certified by peer review) is the author/funder. All rights reserved. No reuse allowed without permission.

Molecular docking enables the analysis of protein-substrate interactions, the assessment of substrate specificity, the evaluation of docking scores, and the optimization of enzyme structures. By predicting binding affinities and stability, molecular docking aids in identifying enzymes with strong substrate binding and high selectivity (Anggraini et al., 2023; Futane et al., 2023; Sahil et al., 2023; Shahbaaz et al., 2018). This computational approach significantly enhances the efficiency of enzyme selection, enabling the development of sensitive and specific biosensors for diverse applications. Additionally, molecular dynamics simulation of docked complexes provides insights into the dynamic behavior of enzyme-substrate interactions, further elucidating the stability and conformational changes crucial for biosensor design and optimization. In the current work, a bioinformatics pipeline was used to screen glucose-specific GBPs from large datasets of proteins acquired from a protein database. Sequence-based analysis was done to filter out unique GBPs and molecular docking and molecular dynamics simulation were employed to screen specific GBPs. A unique set of GBPs with high binding affinity to the glucose molecule were identified.

2. Methodology

The overall methodology employed in this study is illustrated in Figure 1. To screen for glucose binding proteins, a combination of computational tools was utilized.

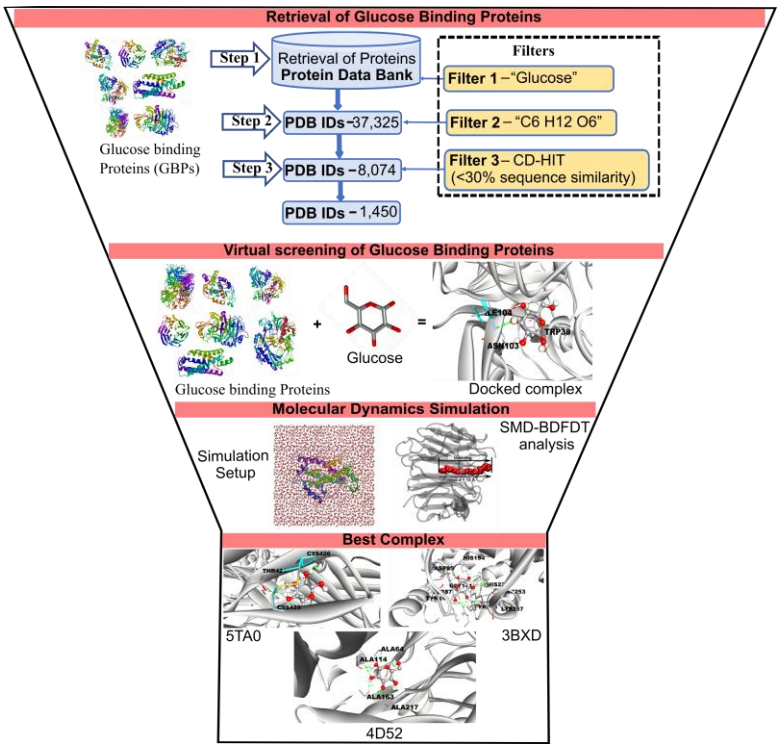

bioRxiv preprint doi: https://doi.org/10.1101/2024.03.20.585966; this version posted March 23, 2024. The copyright holder for this preprint (which was not certified by peer review) is the author/funder. All rights reserved. No reuse allowed without permission.

Figure 1: Schematic of bioinformatics pipeline used to screen the best glucose binding proteins.

2.1 Virtual screening of glucose binding proteins

The 3D structure of glucose (PubChem ID 5793) was retrieved from PubChem database and subsequently prepared by AutoDock4 for docking against filtered GBPs. In the study, glucose-binding proteins were downloaded from the PDB database (Berman et al., 2000) using keyword "glucose" and then filtered out by using two filters (Glucose & Homology filter). Again, Autodock4 was employed for proteins preparation for molecular docking. AutoDock Vina (Trott & Olson, 2009) was employed for protein-ligand docking. The Parallelized Open Babel & Autodock Suite Pipeline (POAP) (Samdani & Vetrivel, 2018) facilitated the automation of docking for multiple proteins and ligands. Discovery Studio Visualizer was used for visualizing protein-ligand interactions (Studio, 2008).

2.2 Filtering and Elimination of redundant GBPs

To optimize computational time and cost, several filters were implemented to eliminate redundant proteins. Redundancy criteria encompassed proteins unrelated to glucose, mutations within the same proteins, and homologous proteins. The integration of these filters facilitated the refinement of our dataset, concentrating exclusively on the most pertinent proteins for our molecular docking experiments.

The filters applied were as follows:

- **Keyword Filter (Filter 1):** Specific search terms such as "glucose" were utilized to identify relevant proteins in the databases.
- **Glucose Filter (Filter 2):** The chemical formula " $C_6H_{12}O_6$" was again employed to identify unique proteins.
- **Homology filter (Filter 3):** Proteins with more than 30% amino acid sequence similarity, indicating homology, were identified through a BLAST search and subsequently removed from dataset (Altschul et al., 1990; Fu et al., 2012).

2.3 Molecular dynamics simulation studies of docked complexes

bioRxiv preprint doi: https://doi.org/10.1101/2024.03.20.585966; this version posted March 23, 2024. The copyright holder for this preprint (which was not certified by peer review) is the author/funder. All rights reserved. No reuse allowed without permission.

The simulation setup of docked complexes was prepared by the CHARMM-GUI solution builder (Lee et al., 2016). Details of the simulation setup are given in table S1. Equilibration and production were conducted under constant volume, pressure, and temperature (1 atm and 310 K) conditions using NAMD 2.14 with CHARMM36m force field(Huang et al., 2017) for the 100ns. Structural changes during the simulation were measured using root mean square deviation (RMSD), with large RMSD values indicating significant motion and low RMSD values indicating a stable system. Trajectories analysis and visualization were performed using VMD (Humphrey et al., 1996).

2.4 SMD-BD-FDT analysis of docked complexes

Steered molecular dynamics (SMD) simulations were conducted using the Brownian dynamics fluctuation-dissipation theorem (BD-FDT) method (Chen, 2008) to accurately determine the free-energy profiles for glucose unbinding from protein-ligand complexes. The most stable structures of protein-ligand complexes were selected from MD simulations. CHARMM36m was utilized as the preferred force field, with a damping coefficient maintained at 5/ps. The vector connecting the center of mass of the glucose molecule to the center of mass of the alpha carbon atoms (within the binding site residues) was chosen as the pulling direction. The pulling speed was set at 0.002 Å/ps, while rotational and translational motion of the protein-ligand complexes were fixed during the simulation. The distance between the bound state and the unbound state was divided into equal segments of 1 Angstrom. Ten forward and reverse paths were sampled for each segment as follows: the system was equilibrated for 0.5 ns with glucose held at the starting point of the segment, then glucose was steered 1 Å away from the binding site to sample a forward path. Subsequently, the system was equilibrated for 0.5 ns with glucose held at the end point of the segment. After equilibration, glucose was steered 1 Å towards the binding site to sample a reverse path. This process was repeated ten times for each segment from the bound state to the dissociated state. The potential of mean force (PMF) was then calculated using these paths from equation (1),

$$exp(-\beta \Delta G) = \frac{\left\langle \exp\left(-\frac{1}{2}\beta W_{A\to B}\right)\right\rangle_F}{\left\langle \exp\left(-\frac{1}{2}\beta W_{B\to A}\right)\right\rangle_R} \qquad (1)$$

bioRxiv preprint doi: https://doi.org/10.1101/2024.03.20.585966; this version posted March 23, 2024. The copyright holder for this preprint (which was not certified by peer review) is the author/funder. All rights reserved. No reuse allowed without permission.

where the BD-FDT relates the equilibrium free energy to the no equilibrium work according to the equation. Here, $W_{A\to B}$ is the force-displacement integral along a forward path from State A to State B, $W_{B\to A}$ is a similarly defined force-displacement integral along a reverse path from State B to State A.

3. Results and discussion

3.1 Filtering of glucose binding proteins

A total of 37,325 hits were identified, indicating a potential association with glucose-binding proteins, using Filter 1. Filter 2, which employed the molecular formula of glucose ($C_6H_{12}O_6$), narrowed down the protein candidates to 8,074 entries. Subsequently, Filter 3 utilized the CD-HIT algorithm to cluster proteins exhibiting high sequence similarity. This process resulted in a refined set of 1,450 proteins, as detailed in **Table S2.**

3.2 Virtual screening of glucose binding proteins

Virtual screening of the selected 1,450 GBPs showed significant variations in their binding affinity with glucose **(Table S3).** The GBPs were arranged in decreasing order of their docking scores, ΔE_{AD}, reflecting their potential binding affinity. Table 1 lists the docking scores for the top five GPB candidate compounds, along with their respective interacting residues and types of interacting bonds. Whereas, Figure 2 shows the three-dimensional structures of these GBPs, Figure 3 shows respective glucose-protein interactions at predicted binding site. The binding site interactions are shown in greater detail in Figure S1. Among the proteins, 5TA0 exhibited the highest docking score (-7.70 kcal/mol), suggesting a strong binding affinity. For comparison, the commonly used GBP, glucose oxidase (1GAL) was also included in the list. In addition, a GBP with a very low binding affinity (-4.9 kcal/mol), human glycolipid transfer protein (2EVL), was included as a negative control.

Table 1: Table represent a comprehensive overview of the ligand-protein complexes, along with essential information such as their respective PDB IDs with name, the interacting residues involved in the binding, and the types of bonds formed between the ligands and proteins.

bioRxiv preprint doi: https://doi.org/10.1101/2024.03.20.585966; this version posted March 23, 2024. The copyright holder for this preprint (which was not certified by peer review) is the author/funder. All rights reserved. No reuse allowed without permission.

S. No.	Protein-glucose complex	Docking score (kcal/mol)	Interacting residues	Types of interacting bonds
1	5TA0 (Glycoside Hydrolase)	-7.70	ARG B:589, MET B:352, GLU B:356, CYS B:433, THR B:424, ASN B:425, ILE B:431, PRO B:429, CYS B:426, ASP B:427	van der Waals, Conventional Hydrogen Bond
2	3BXD (Myo-inositol oxygenase)	-7.30	TYR A:31,PRO A:89,TYR A:44,ARG A:29,TYR A:223,LEU A:254,ASP A:88,SER A:87,ASP A:142,LYS A:257,ASP A:85,VAL A:140,ASP A:253,GLY A:141,LYS A:127,HIS A:194,HIS A:220,ASP A:124,SER A:221	van der Waals, Conventional Hydrogen Bond, Carbon Hydrogen Bond, Unfavorable Donor-Donor
3	4D52 (*Aspergillus fumigatus lectin*)	-7.13	ALA C:17, ILE C:15, ALA C:16, VAL C:62, ILE C:215, ALA C:216, ILE C:161, ILE C:112, ALA C:63, GLY C:162, THR C:65, ALA C:217, ALA C:64, ALA C:114, ALA C:113, ALA C:163, VAL C:115	van der Waals, Conventional Hydrogen Bond
4	2O7I (Thermophilic cellobiose binding protein)	-7.13	TYR A:299,TRP A:384,TRP A:381,ASP A:383,THR A:382,TRP A:511,ASN A:216,PHE A:234,TRP A:536,LEU A:233,GLY A:232,TRP A:16, GLY A:13	van der Waals, Conventional Hydrogen Bond, Unfavorable Donor-Donor
5	4V20 (Cellobiohydrolase)	-7.00	TYR A:82,ASN A:103,ILE A:104,ASN A:200,LYS A:181,TRP A:38,ASN A:37, ALA A:201	van der Waals, Conventional Hydrogen Bond, Unfavorable Acceptor-Acceptor, Pi-Sigma
6	1GAL (Glucose Oxidase)	-6.7	VAL A:106, SER A:103, PHE A:564, ARG A:95, SER A:96, LEU A:105, SER A:291, GLY A:102, GLY A:97, LEU A:29, THR A:104, SER A:51, GLY A:101, HIS A:78, GLY A:549, THR A:30, TYR A:80, ASP A:548,	van der Waals, Conventional Hydrogen Bond, Unfavorable Acceptor-Acceptor

bioRxiv preprint doi: https://doi.org/10.1101/2024.03.20.585966; this version posted March 23, 2024. The copyright holder for this preprint (which was not certified by peer review) is the author/funder. All rights reserved. No reuse allowed without permission.

			GLY A:28, VAL A:293, ASN A:98, GLY A:99, ALA A:288, GLY A:290, GLY A:31, ALA A:228, ALA A:289, GLU A:50, GLY A:26, SER A:294, GLY A:27, LEU A:32, ALA A:25	
7	2EVL (Human Glycolipid Transfer Protein)	-4.9	LEU A:37, ILE A:124, PHE A:107, ASN A:127, PRO A:156, ALA A:128, ARG A:125, ALA A:131, PHE A:42, PHE A:34, PHE A:103, PHE A:161, ALA A:154, ALA A:151, ALA A:155, LEU A:152, TYR A:153, ALA A:150, PHE A:148 , GLN A:149, TYR A:132, ILE A:45, VAL A:41, LEU A:136, ILE A:147	van der Waals, Unfavorable Acceptor-Acceptor

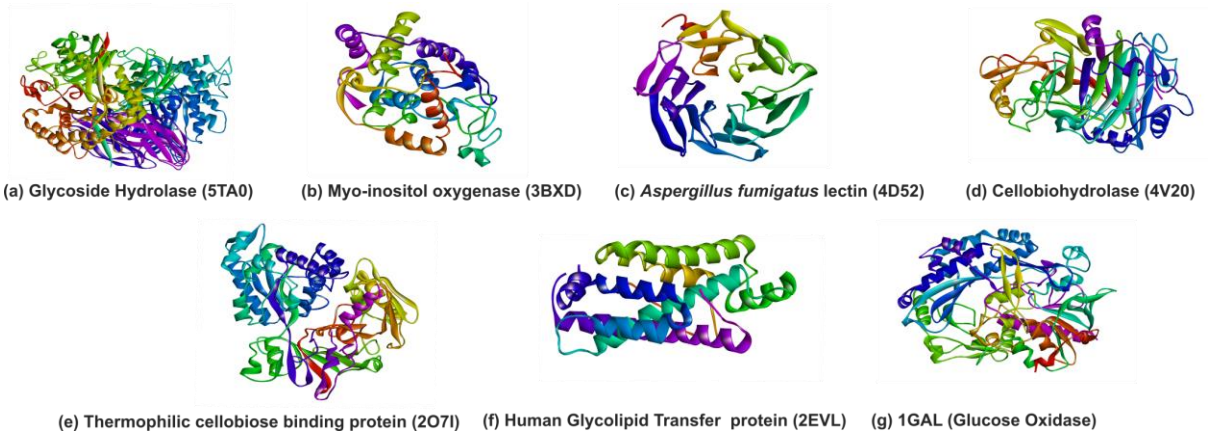

Figure 2: Glucose-binding proteins (GBPs) identified through molecular docking screening. The proteins are labeled as follows: (a) Glycoside Hydrolase (5TA0), (b) Myo-inositol oxygenase (3BXD), (c) *Aspergillus fumigatus* lectin (4D52), (d) Cellobiohydrolase (4V20), (e) Thermophilic cellobiose binding protein (2O7I), (f) Human Glycolipid Transfer Protein (2EVL), and (g) Glucose Oxidase (1GAL).

bioRxiv preprint doi: https://doi.org/10.1101/2024.03.20.585966; this version posted March 23, 2024. The copyright holder for this preprint (which was not certified by peer review) is the author/funder. All rights reserved. No reuse allowed without permission.

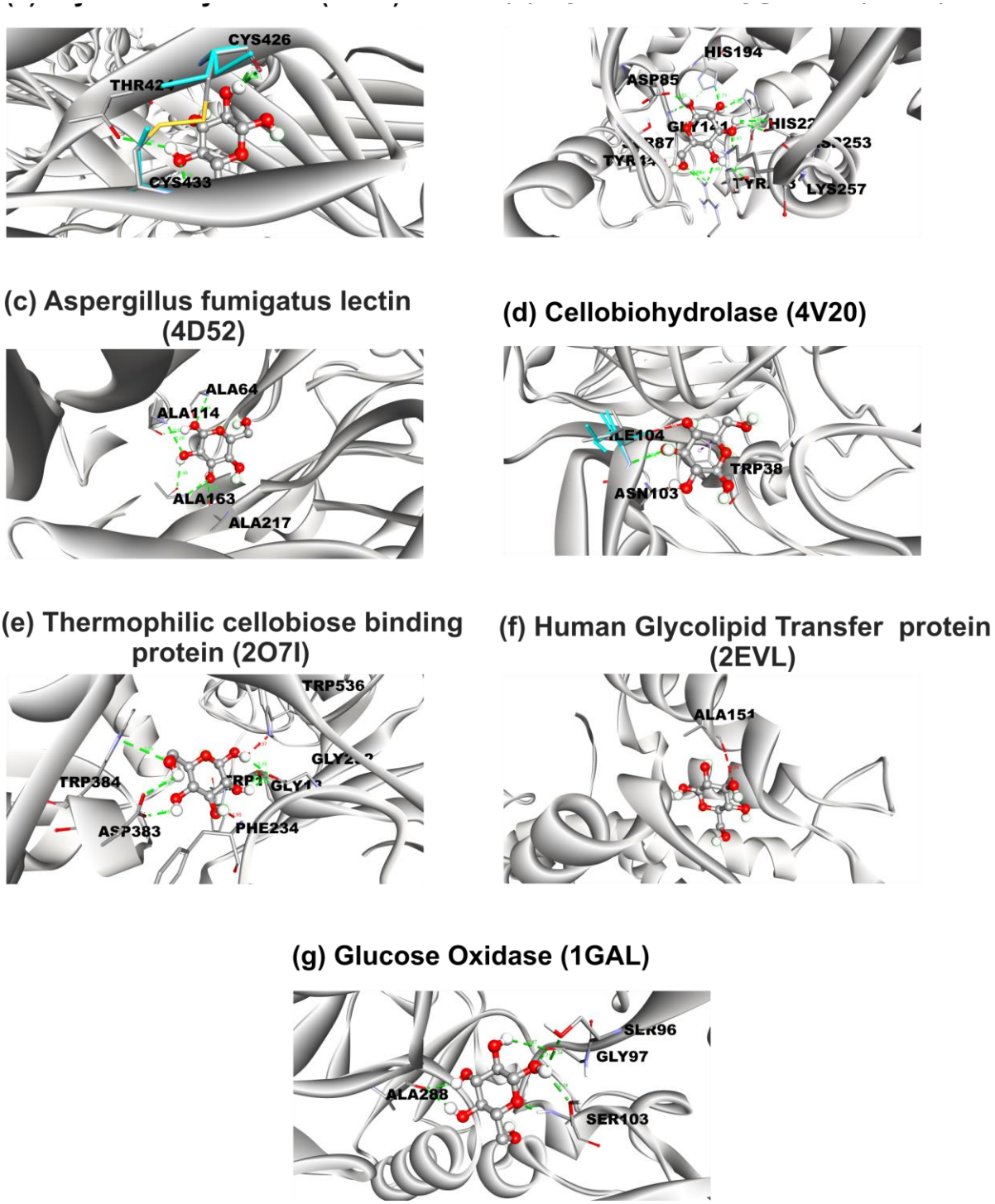

Figure 3: Visualization of intermolecular interactions using Discovery Studio Visualizer. The 2D plot showcases the interactions in (a) Glycoside Hydrolase (5TA0), (b) Myo-inositol oxygenase (3BXD), (c) *Aspergillus fumigatus* lectin (4D52), (d) Cellobiohydrolase (4V20), (e) Thermophilic cellobiose binding protein (2O7I), (f) Human Glycolipid Transfer Protein (2EVL), and (g) Glucose Oxidase (1GAL). Dashed lines indicate various interaction types,

bioRxiv preprint doi: https://doi.org/10.1101/2024.03.20.585966; this version posted March 23, 2024. The copyright holder for this preprint (which was not certified by peer review) is the author/funder. All rights reserved. No reuse allowed without permission.

with each color representing a specific interaction type. Residues are depicted with their three-letter code and residue number.

3.3 Simulation of docked complexes

The stability of the docked complexes (candidate protein + glucose) and associated structural changes were monitored with 100 ns long MD simulations (Figure 4a). RMSD values for all docked complexes were found to vary between 1 – 6 (Å). RMSD values for the 4D52 complex were the most stable among the seven GBPs (Figures 4b, c). In addition, 4V20 and 3BXD complexes also demonstrated higher stability compared to the rest of the complexes. The 2O7I complex exhibited relatively higher RMSD values compared to the other docked complexes. Hydrogen bond occupancy was calculated for all protein-ligand complexes, revealing varying degrees of hydrogen bond occupancy for each complex (Figure S2). These results suggested that RMSD values alone may not be the primary determinant of GBP complex stability.

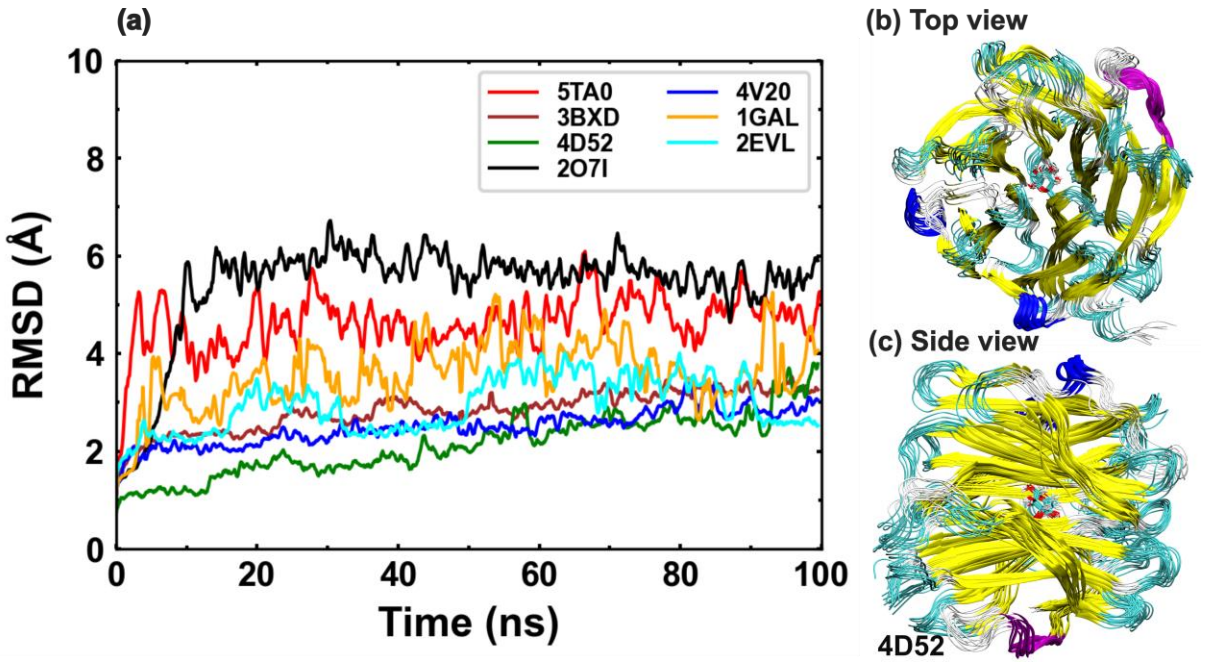

Figure 4: (a) Comparative RMSD analysis of the docked protein-glucose complexes, providing illuminating observations on their remarkable stability and conformational dynamics throughout the molecular dynamics (MD) simulation. **(b, c)** Different conformation of glucose (represented by licorice) and protein (represented by cartoon) during simulation time.

bioRxiv preprint doi: https://doi.org/10.1101/2024.03.20.585966; this version posted March 23, 2024. The copyright holder for this preprint (which was not certified by peer review) is the author/funder. All rights reserved. No reuse allowed without permission.

However, not all complexes remained stable during the simulations. The distance of the glucose molecule from the binding sites (CA atom) of GBPs, d_G, was used as a measure of the integrity of the GBP-glucose complex. Plots of variation of d_G with time are shown in Figures 5a, b. A residence time, τ_b, for a specific GBP was defined as the time after which the corresponding d_G value started diverging significantly from its initial value. Based on τ_b values (estimated from the d_G versus time plots), the seven GBPs were characterized as candidates with either strong (Figure 5a) or weak (Figure 5b) binding affinities. Whereas, 4D52 and 1GAL demonstrated strong binding affinities, 4V20, 2O7I, and 2EVL showed the weakest binding with glucose. Complexes of 3BXD and 5TA0 remained bound to glucose for approximately 35 ns and 70 ns, respectively. Since these complexes remained stable for much longer when compared to the weakly-binding GBPs, they were also classified as strongly-binding GBPs. The residence time, estimated from these calculations, was used as a parameter in the selection process, because it describes the dynamics of ligand binding to the GBP. Glucose binding/unbinding times of a strongly-binding (5TA0) and a weakly-binding (2EVL) GBPs are shown in Figures 5c and d, respectively.

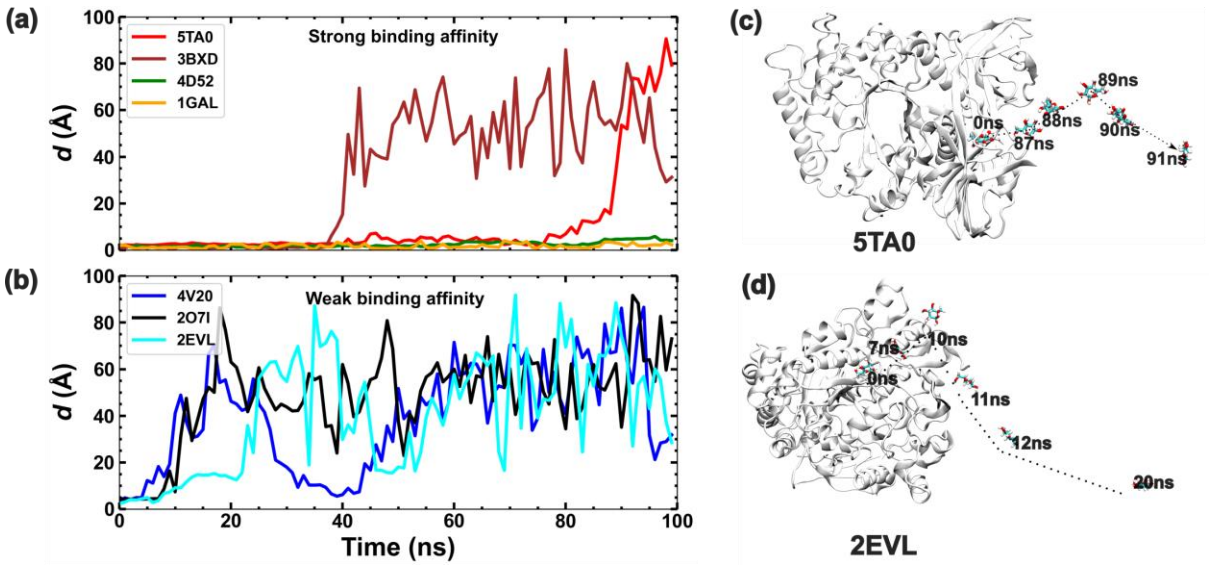

Figure 5: (a-b) The graph displays the ligand behavior and distance from the binding site throughout the simulation duration. **(c-d)** Illustration depicting the stability of glucose with 5TA0 and the instability of glucose with 2EVL protein over the course of the simulation.

bioRxiv preprint doi: https://doi.org/10.1101/2024.03.20.585966; this version posted March 23, 2024. The copyright holder for this preprint (which was not certified by peer review) is the author/funder. All rights reserved. No reuse allowed without permission.

3.4 Potential of mean force from SMD-BD-FDT

Using the SMD-BD-FDT simulations, potential of mean force (PMF) curves, for the seven GBPs, were estimated as a function of the distance of the ligand from the binding site, ξ (Figure 6). The binding free energy of a ligand-protein complex was inferred from the PMF curve as the depth of the potential well. Most of the BD-FDT binding energy values, ΔG_b, were different from the binding energies estimated from the AutoDock values (Figure 7). For instance, BD-FDT predicted a binding energy of -16.7 kcal/mol for 5TAO which was significantly higher than the value of -7.7 kcal/mol estimated from AutoDock. Interestingly, 2EVL, which was selected for its low binding score displayed a low binding energy value of -2.6 kcal/mol in the BD-FDT simulations as well. Moreover, 2O7I demonstrated a binding free energy of -11.5 kcal/mol, higher than the docking prediction of -7.13 kcal/mol. However, the PMF curve showed a negative curvature indicating weak binding of glucose with the protein. This inference is consistent with the extremely short τ_b for 2O7I (Figure 5c) and in conflict with the prediction of a stable glucose-2O7I complex from AutoDock. It shows that AutoDock scores for binding energies may not capture all dynamical aspects of ligand binding to the GBP. Hence, AutoDock predictions need to be guided by more rigorous physics-based simulations to generate rules for protein selection. Representative paths corresponding to glucose unbinding for each GBP are shown in Figure S3.

The examination of individual cases further emphasized the diverse characteristics of the complexes. The analysis of the potential of 4V20 elucidated its limited binding capacity, supported by a shallow well and subsequent dissociation, confirmed by a low PMF value. Similarly, 2EVL showed weakened bonding, as evidenced by the shallow well and subsequent unbinding of glucose beyond a certain threshold. On the other hand, the unbinding pathways of 2O7I and 1GAL revealed distinct patterns, reflecting the complexities of their interactions. While 2O7I demonstrated a relatively abrupt dissociation, 1GAL displayed an intermediate state during the process, ultimately leading to complete detachment. Notably, 5TA0 exhibited unique unbinding patterns characterized by distinct potential wells and intermediate states, underscoring the intricate nature of their binding mechanisms. Figure 7 compares binding energy predictions from docking, ΔE_{AD}, with those from SMD simulations, ΔG_b. Both ΔE_{AD} and ΔG_b values were the highest for 5TA0. Other proteins with high ΔE_{AD} scores (3BXD, 4D52, and 1GAL) also demonstrated high ΔG_b values. For 2EVL, a weakly-binding GBP, both ΔE_{AD} and ΔG_b values were low. These observations indicated a relatively strong correlation between ΔE_{AD} and ΔG_b values. They also set the stage for finding other correlations between energy-

bioRxiv preprint doi: https://doi.org/10.1101/2024.03.20.585966; this version posted March 23, 2024. The copyright holder for this preprint (which was not certified by peer review) is the author/funder. All rights reserved. No reuse allowed without permission.

minimization based AutoDock predictions and more detailed atomistic MD simulations. Such correlations can assist in developing a rational GBP selection framework based on relatively quicker, albeit approximate, docking simulations.

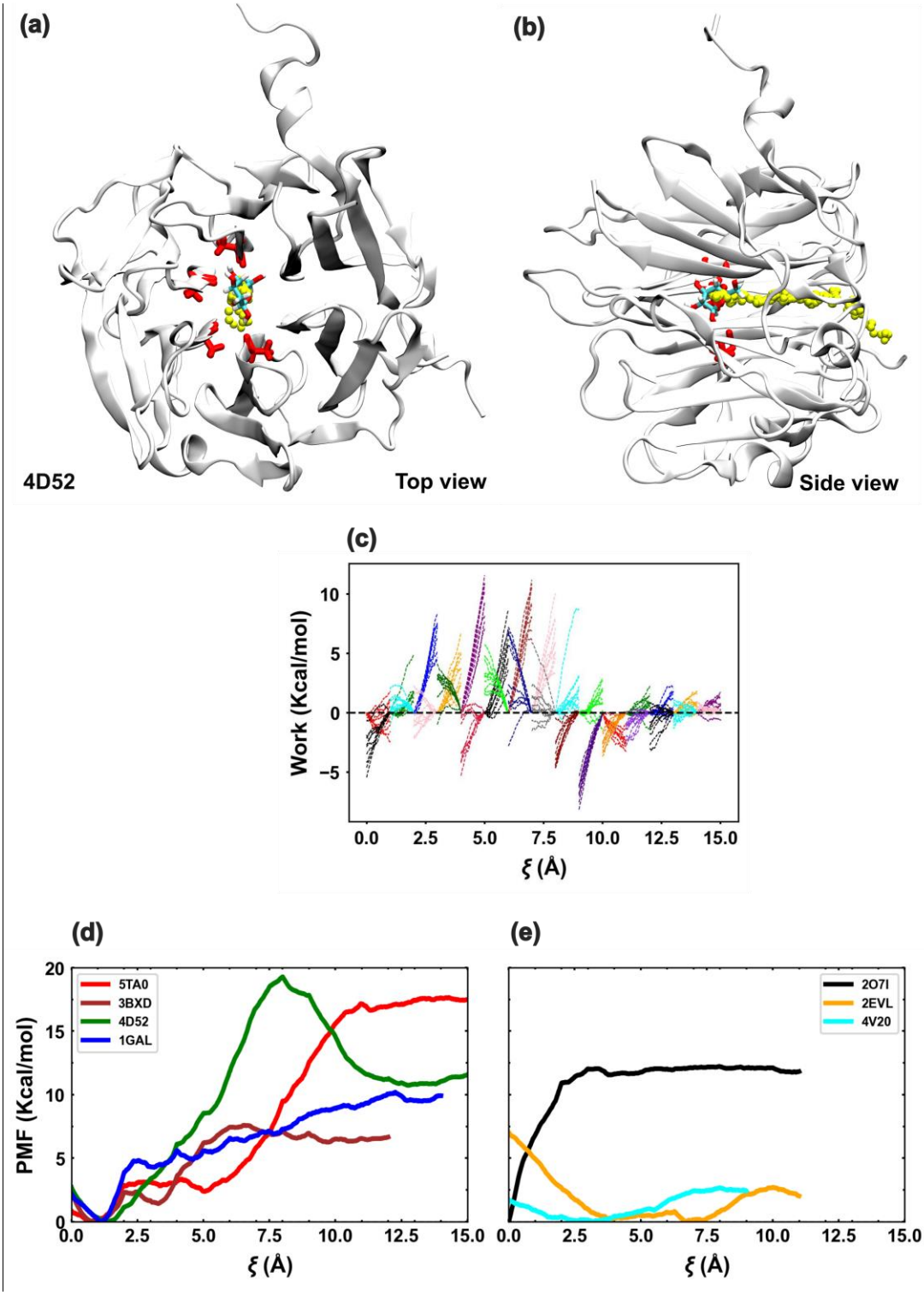

Figure 6: (a) Top view; (b) Side view of proteins with binding sites and ligand. The figure illustrates the glucose binding site in line representation, glucose in licorice representation, and

bioRxiv preprint doi: https://doi.org/10.1101/2024.03.20.585966; this version posted March 23, 2024. The copyright holder for this preprint (which was not certified by peer review) is the author/funder. All rights reserved. No reuse allowed without permission.

the pathway indicated in beads representation in yellow color. **(b)** Work done along the forward (spreading out towards right) and reverse (spreading out towards left) pulling paths **(c-d)** PMF profile of GBPs with glucose during the binding process.

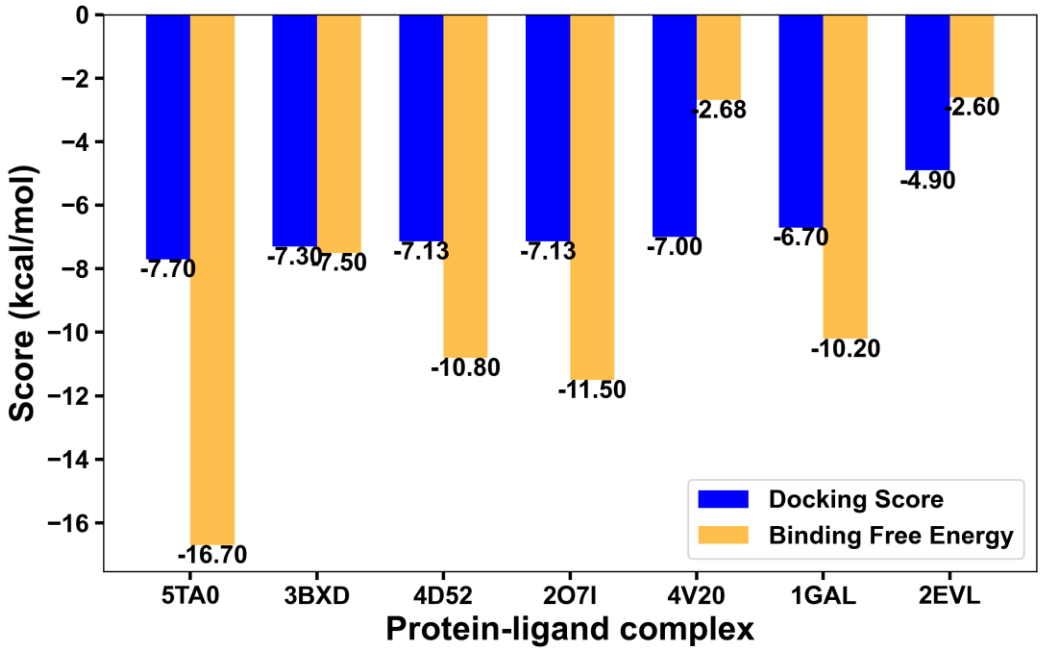

Figure 7: Bar plot showing docking score and binding free energy of protein ligand complexes.

3.5 Correlating docking predictions with MD simulations

A comprehensive analysis was carried out to correlate results from docking with those from MD simulations. It should be noted that absolute values of the binding energies, $|\Delta G_b|$ and $|\Delta E_{AD}|$ are represented in these plots. Key parameters derived from MD simulations, including glucose residence time (τ_b), glucose binding free energy ($|\Delta G_b|$), and the hydrogen bond occupancy (n_{HBD}), were selected as the first set of parameters. The second set of parameters, derived from docking simulations, included the docking energy ($|\Delta E_{AD}|$), cavity depth of the binding site from the GBP surface (d_c) and the number of hydrogen bonds between glucose and GBP residues (n_{AD}). Correlations were sought between parameters in the first set with those in the second set. Figures 8a – c plot τ_b as a function of the docking parameters from the second set. Similarly, Figures 8d – f plot $|\Delta G_b|$ as a function of the second set docking parameters.

bioRxiv preprint doi: https://doi.org/10.1101/2024.03.20.585966; this version posted March 23, 2024. The copyright holder for this preprint (which was not certified by peer review) is the author/funder. All rights reserved. No reuse allowed without permission.

Whereas, τ_b did not show any correlation with either $|\Delta E_{AD}|$ or n_{AD} (Figures 8a,c), it showed a strong linear correlation with d_c (Figure 8b). The correlation plot of τ_b vs d_c showed that a large cavity depth resulted in a strongly-bound and stable glucose-GBP complexes. A comparison with MD results from Figures 5a and b indicated that weakly-bound GBPs (2EVL, 4V20 and 2O7I) had $d_c < 10$Å. Interestingly, both 4V20 and 2O7I had high $|\Delta E_{AD}|$ values, implying that a high docking score may not necessarily lead to stable glucose-GBP complexes.

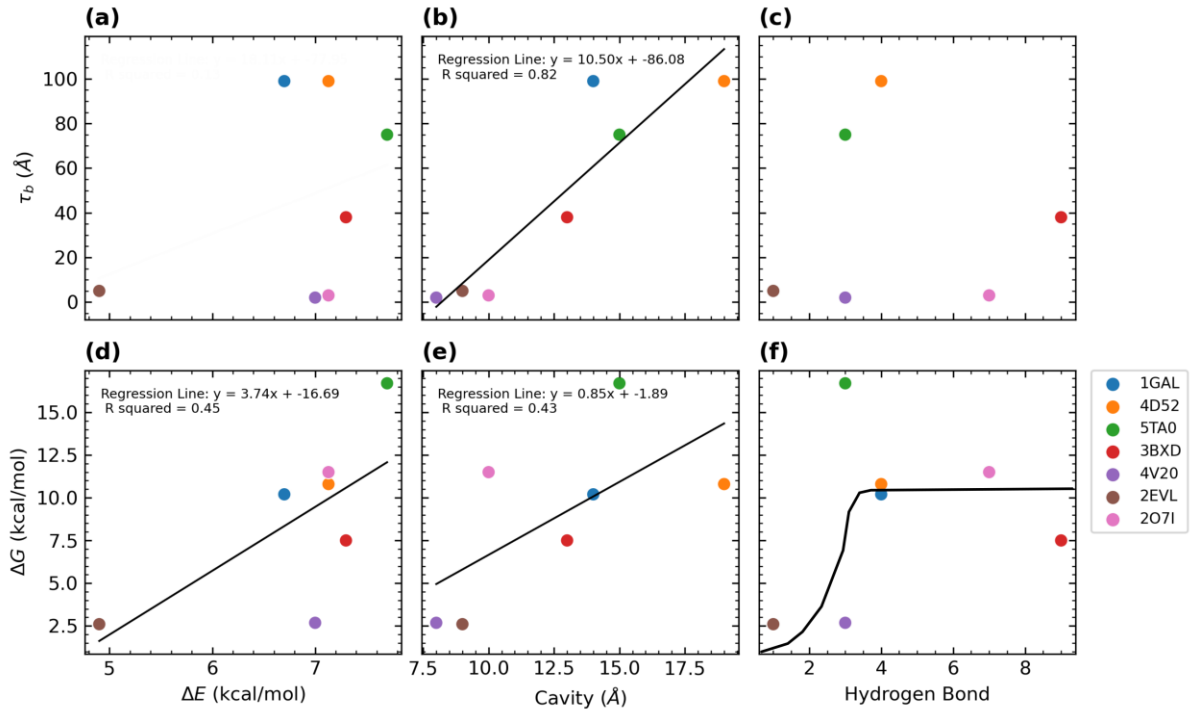

Figure 8: Correlation plot between ΔG, ΔE, hydrogen bond, cavity(Å) and τ_b (Å)

The binding free energy, $|\Delta G_b|$, showed stronger correlations with the three docking parameters (Figures 8d – f). It increased almost linearly with increasing value of both $|\Delta E_{AD}|$ (Figure 8d), but there were a couple of anomalies. As stated above, 4V20 had a high $|\Delta E_{AD}|$ but did not form a stable complex (Figure 5b) because of which it had a low $|\Delta G_b|$ value. Similarly, 2O7I also formed an unstable complex (though it had a high $|\Delta E_{AD}|$, but a high $|\Delta G_b|$ value was interpreted from its anomalous PMF curve in Figure 6e. Again, $|\Delta G_b|$ showed a linear correlation with d_c (Figure 8e). In general, GBPs with deeper cavities resulted in higher $|\Delta G_b|$ values. Thus, cavity depth emerged as a reliable indicator of glucose binding with a GBP. The correlation plots in Figures 8b,e suggested that stable glucose-GBP complexes emerged for $d_c > 12$Å. Plotting the variation of $|\Delta G_b|$ with respect to n_{AD} provided insight into the effect of bonding environment at the ligand binding site on the stability of the glucose-GBP complex.

bioRxiv preprint doi: https://doi.org/10.1101/2024.03.20.585966; this version posted March 23, 2024. The copyright holder for this preprint (which was not certified by peer review) is the author/funder. All rights reserved. No reuse allowed without permission.

A sigmoidal dependence of $|\Delta G_b|$ with respect to n_{AD} was inferred from Figure 8f. Whereas, GBPs with $n_{AD} \leq 3$ corresponded to low $|\Delta G_b|$ values (weakly-binding), GBPs with $n_{AD} > 3$ corresponded to stable complexes with ΔG_b values close to 10 kcal/mol. Thus, $|\Delta G_b|$ versus n_{AD} plot indicated a threshold value of $n_{AD} = 3$, above which stable complexes could be found. To validate these correlations interpreted from Figure 8, $|\Delta G_b|$ was plotted with respect to two other parameters also obtained from MD data, namely, n_{HBD} and τ_b (Figure 9). The plot of $|\Delta G_b|$ with respect to n_{HBD} showed a sigmoidal behavior similar to the plot in Figure 8f, indicating that a certain minimum number of hydrogen bonds (at the binding site) are required for stable glucose-GBP complexes. Similarly, low τ_b values corresponded to low $|\Delta G_b|$ values and by extension a weakly-bound glucose molecule (Figure 9b).

Thus, the correlation plots in Figure 8 helped in arriving at a set of docking parameters that would reliably predict GBPs that bound strongly to glucose. Using these parameters would make the protein selection process more efficient since these parameters would be obtained from relatively faster docking simulations. Based on the above discussion, a combination threshold values of $|\Delta E_{AD}|$, d_c and n_{AD} can be used to reliably predict candidate GBPs. Specifically, a GBP with docking parameters corresponding to $|\Delta E_{AD}| > 7.0$, $d_c > 12$Å and $n_{AD} > 3$ should result in the formation of a stable glucose-protein complex.

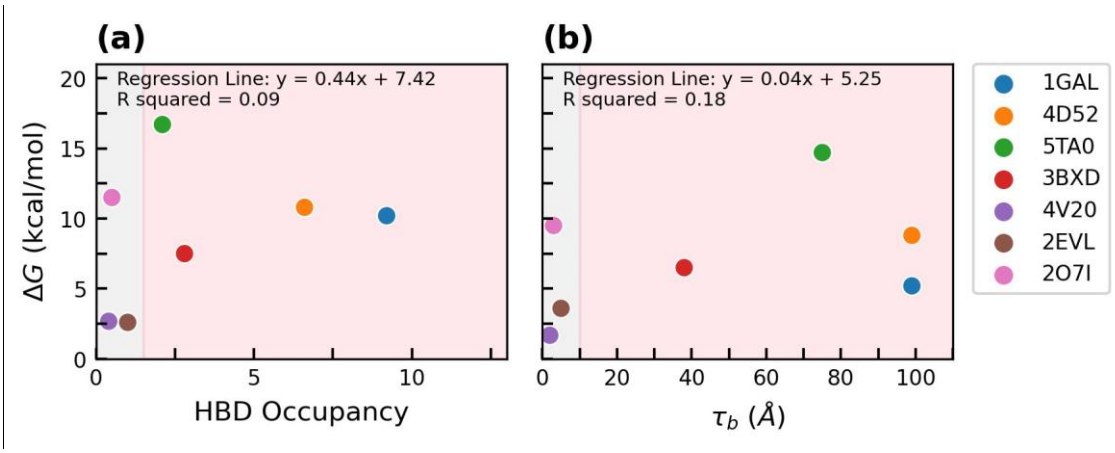

Figure 9: Correlation plot between ΔG, HBD occupancy, and τ_b (Å). 2O7I, 2EVL, and 2O7I with lowest HBD occupancy and τ_b (Å) values shown in light grey color, 1GAL, 4D52, 5TA0 and 3BXD with high HBD occupancy and τ_b (Å) values shown in light pink color.

Figure 10 is a flowchart that outlines a "GBP selection pipeline" that incorporates the above-mentioned selection rules (based only on docking data) and few test MD simulations. It comprises the following steps,

i. Use Filters 1, 2 and 3 to select candidates from the database

bioRxiv preprint doi: https://doi.org/10.1101/2024.03.20.585966; this version posted March 23, 2024. The copyright holder for this preprint (which was not certified by peer review) is the author/funder. All rights reserved. No reuse allowed without permission.

ii. Apply threshold values of $|\Delta E_{AD}| > 7.0$ kcal/mol, $d_c > 12$Å and $n_{AD} > 3$ to arrive at potentially strongly-binding GBPs

iii. Computational validation of selection process: Conduct short (100 ns) MD simulations on a small sample of proteins (≈10 proteins) to test stability of glucose-protein complex (along the lines of Figure 5)

iv. Experimental validation: Use top candidates for further experimental binding studies

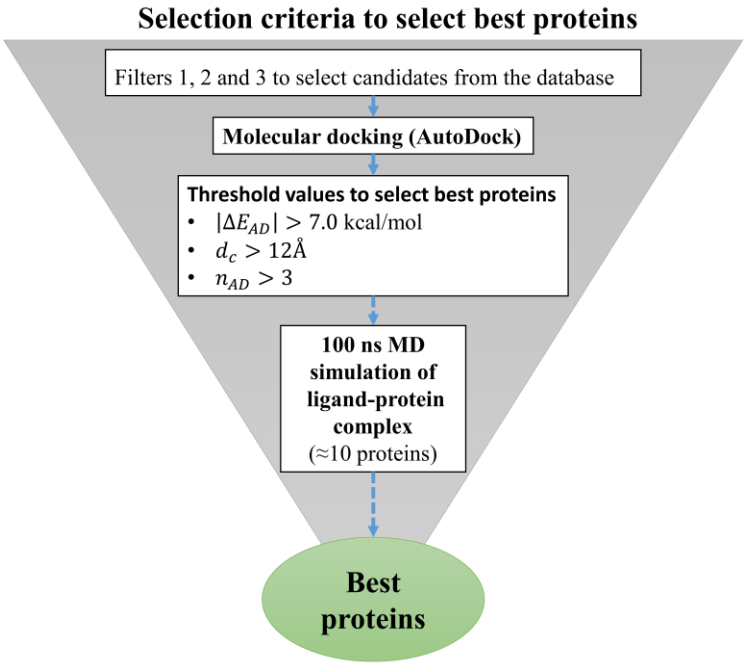

Figure 10: Flow chart showing selection criteria for best proteins

4. Conclusion

Biosensors are valuable tools for monitoring the quality of fruit juices due to their fast response time, portability, and cost-effectiveness. Enzymatic biosensors have proven successful due to their high specificity and low manufacturing cost. In the current work, unique glucose-binding proteins were identified by using a bioinformatics pipeline including sequence-based analysis, molecular docking, and MD simulations. A total of 37,325 GBP hits were identified from PDB database, and subsequently, a total of 1450 unique GBPs were found suitable. After virtual screening, 5TA0 (Glycoside Hydrolase), 3BXD (Myo-inositol oxygenase), and 4D52 (*Aspergillus fumigatus* lectin) exhibited the highest binding affinities, with values of -7.70, -7.30, and -7.13 kcal/mol, respectively. Conventional MD simulations and SMD BD-FDT simulations revealed the binding and unbinding mechanisms of the ligand-protein complex, suggesting that 5TA0 demonstrated the best binding affinity and binding free energy. These

bioRxiv preprint doi: https://doi.org/10.1101/2024.03.20.585966; this version posted March 23, 2024. The copyright holder for this preprint (which was not certified by peer review) is the author/funder. All rights reserved. No reuse allowed without permission.

findings provide insights into the potential of these protein complexes for developing improved biosensors for measuring glucose content in fruit juices.

Acknowledgments

The authors acknowledge to IIT Bombay for providing HPC facility.

Disclosure statement

No potential conflict of interest was reported by the author(s).

Funding

There are no funding sources to declare.

Author's Contributions

#Authors have equally contributed.

References

Altschul, S. F., Gish, W., Miller, W., Myers, E. W., & Lipman, D. J. (1990). Basic local alignment search tool. *Journal of Molecular Biology*, *215*(3), 403–410. https://doi.org/10.1016/S0022-2836(05)80360-2

Anggraini, L. E., Rahmawati, I., Nasution, M. A. F., Jiwanti, P. K., Einaga, Y., & Ivandini, T. A. (2023). Development of an Acrylamide Biosensor Using Guanine and Adenine as Biomarkers at Boron-Doped Diamond Electrodes: Integrated Molecular Docking and Experimental Studies. *Https://Doi.Org/10.1246/Bcsj.20230030*, *96*(5), 420–428. https://doi.org/10.1246/BCSJ.20230030

Bag, S., & Mandal, D. (2023). Overview of Biosensors and Its Application in Health Care. *Smart Innovation, Systems and Technologies*, *322*, 29–60. https://doi.org/10.1007/978-981-19-7107-5_3/COVER

Bankar, S. B., Bule, M. V., Singhal, R. S., & Ananthanarayan, L. (2009). Glucose oxidase--an overview. *Biotechnology Advances*, *27*(4), 489–501. https://doi.org/10.1016/J.BIOTECHADV.2009.04.003

bioRxiv preprint doi: https://doi.org/10.1101/2024.03.20.585966; this version posted March 23, 2024. The copyright holder for this preprint (which was not certified by peer review) is the author/funder. All rights reserved. No reuse allowed without permission.

Berman, H. M., Westbrook, J., Feng, Z., Gilliland, G., Bhat, T. N., Weissig, H., Shindyalov, I. N., & Bourne, P. E. (2000). The Protein Data Bank. In *Nucleic Acids Research* (Vol. 28, Issue 1, pp. 235–242). Oxford University Press. https://doi.org/10.1093/nar/28.1.235

Butt, M. A., Kazanskiy, N. L., Khonina, S. N., Voronkov, G. S., Grakhova, E. P., & Kutluyarov, R. V. (2023). A Review on Photonic Sensing Technologies: Status and Outlook. *Biosensors 2023, Vol. 13, Page 568*, *13*(5), 568. https://doi.org/10.3390/BIOS13050568

Chadha, U., Bhardwaj, P., Agarwal, R., Rawat, P., Agarwal, R., Gupta, I., Panjwani, M., Singh, S., Ahuja, C., Selvaraj, S. K., Banavoth, M., Sonar, P., Badoni, B., & Chakravorty, A. (2022). Recent progress and growth in biosensors technology: A critical review. *Journal of Industrial and Engineering Chemistry*, *109*, 21–51. https://doi.org/10.1016/J.JIEC.2022.02.010

Chen, L. Y. (2008). Nonequilibrium fluctuation-dissipation theorem of Brownian dynamics. *Journal of Chemical Physics*, *129*(14). https://doi.org/10.1063/1.2992153/187218

Fu, L., Niu, B., Zhu, Z., Wu, S., & Li, W. (2012). CD-HIT: accelerated for clustering the next-generation sequencing data. *Bioinformatics*, *28*(23), 3150–3152. https://doi.org/10.1093/BIOINFORMATICS/BTS565

Futane, A., Narayanamurthy, V., Rao Gannapathy, V., Jadhav, P., Swee Leong, K., & Author, C. (2023). Emerging Trends In Computational Biosensors: Challenges And Future Directions. *Journal of Survey in Fisheries Sciences*, *10*(1), 2888–2905. https://doi.org/10.53555/SFS.V10I1.1280

Guilbault, G. G., & Lubrano, G. J. (1973). An enzyme electrode for the amperometric determination of glucose. *Analytica Chimica Acta*, *64*(3), 439–455. https://doi.org/10.1016/S0003-2670(01)82476-4

Huang, J., Rauscher, S., Nawrocki, G., Ran, T., Feig, M., De Groot, B. L., Grubmüller, H., & MacKerell, A. D. (2017). CHARMM36m: an improved force field for folded and intrinsically disordered proteins. *Nature Methods*, *14*(1), 71–73. https://doi.org/10.1038/NMETH.4067

Humphrey, W., Dalke, A., & Schulten, K. (1996). VMD: Visual molecular dynamics.

bioRxiv preprint doi: https://doi.org/10.1101/2024.03.20.585966; this version posted March 23, 2024. The copyright holder for this preprint (which was not certified by peer review) is the author/funder. All rights reserved. No reuse allowed without permission.

Journal of Molecular Graphics, *14*(1), 33–38. https://doi.org/10.1016/0263-7855(96)00018-5

Kaczmarek, J. A., & Prather, K. L. J. (2021). Effective use of biosensors for high-throughput library screening for metabolite production. *Journal of Industrial Microbiology & Biotechnology*, *48*(9–10), 49. https://doi.org/10.1093/JIMB/KUAB049

Klonoff, D. C. (1997). Noninvasive blood glucose monitoring. *Diabetes Care*, *20*(3), 433–437. https://doi.org/10.2337/DIACARE.20.3.433

Larin, K. V., Eledrisi, M. S., Motamedi, M., & Esenaliev, R. O. (2002). Noninvasive blood glucose monitoring with optical coherence tomography: a pilot study in human subjects. *Diabetes Care*, *25*(12), 2263–2267. https://doi.org/10.2337/DIACARE.25.12.2263

Lee, J., Cheng, X., Swails, J. M., Yeom, M. S., Eastman, P. K., Lemkul, J. A., Wei, S., Buckner, J., Jeong, J. C., Qi, Y., Jo, S., Pande, V. S., Case, D. A., Brooks, C. L., MacKerell, A. D., Klauda, J. B., & Im, W. (2016). CHARMM-GUI Input Generator for NAMD, GROMACS, AMBER, OpenMM, and CHARMM/OpenMM Simulations Using the CHARMM36 Additive Force Field. *Journal of Chemical Theory and Computation*, *12*(1), 405–413. https://doi.org/10.1021/ACS.JCTC.5B00935/ASSET/IMAGES/LARGE/CT-2015-00935E_0005.JPEG

MacKenzie, H. A., Ashton, H. S., Spiers, S., Shen, Y., Freeborn, S. S., Hannigan, J., Lindberg, J., & Rae, P. (1999). Advances in Photoacoustic Noninvasive Glucose Testing. *Clinical Chemistry*, *45*(9), 1587–1595. https://doi.org/10.1093/CLINCHEM/45.9.1587

Pullano, S. A., Greco, M., Bianco, M. G., Foti, D., Brunetti, A., & Fiorillo, A. S. (2022). Glucose biosensors in clinical practice: principles, limits and perspectives of currently used devices. *Theranostics*, *12*(2), 493. https://doi.org/10.7150/THNO.64035

Rabinovitch, B., March, W. F., & Adams, R. L. (1982). Noninvasive glucose monitoring of the aqueous humor of the eye: Part I. Measurement of very small optical rotations. *Diabetes Care*, *5*(3), 254–258. https://doi.org/10.2337/DIACARE.5.3.254

Rassel, S., Xu, C., Zhang, S., & Ban, D. (2020). Noninvasive blood glucose detection using a

bioRxiv preprint doi: https://doi.org/10.1101/2024.03.20.585966; this version posted March 23, 2024. The copyright holder for this preprint (which was not certified by peer review) is the author/funder. All rights reserved. No reuse allowed without permission.

quantum cascade laser. *Analyst*, *145*(7), 2441–2456. https://doi.org/10.1039/c9an02354b

Richiardi, J., Achard, S., Bunke, H., & Ville, D. Van De. (2013). Machine Learning with Brain Graphs: Predictive Modeling Approaches for Functional Imaging in Systems Neuroscience. *IEEE Signal Processing Magazine*, *30*(3), 58–70. https://doi.org/10.1109/MSP.2012.2233865

Sahil, M., Singh, J., Sahu, S., Pal, S. K., Yadav, A., Anand, R., & Mondal, J. (2023). Identifying Selectivity Filters in Protein Biosensor for Ligand Screening. *JACS Au*. https://doi.org/10.1021/JACSAU.3C00374

Samdani, A., & Vetrivel, U. (2018). POAP: A GNU parallel based multithreaded pipeline of open babel and AutoDock suite for boosted high throughput virtual screening. *Computational Biology and Chemistry*, *74*, 39–48. https://doi.org/10.1016/J.COMPBIOLCHEM.2018.02.012

Shahbaaz, M., Kanchi, S., Sabela, M., & Bisetty, K. (2018). Structural basis of pesticide detection by enzymatic biosensing: a molecular docking and MD simulation study. *Journal of Biomolecular Structure and Dynamics*, *36*(6), 1402–1416. https://doi.org/10.1080/07391102.2017.1323673

Singh, S., Kumar, V., Dhanjal, D. S., Datta, S., Prasad, R., & Singh, J. (2020). Biological Biosensors for Monitoring and Diagnosis. *Microbial Biotechnology: Basic Research and Applications*, 317. https://doi.org/10.1007/978-981-15-2817-0_14

Studio, D. (2008). Discovery studio. *Accelrys [2.1]*. https://www.researchgate.net/profile/Tanweer-Alam-2/post/hi_can_somebody_plz_tell_me_how_to_import_a_database_into_Discovery_Studio_for_a_3D_database_search/attachment/59d63bb879197b8077998bbd/AS%3A412232203685889%401475295224962/download/ds-overview-20.pdf

Trott, O., & Olson, A. J. (2009). AutoDock Vina: Improving the speed and accuracy of docking with a new scoring function, efficient optimization, and multithreading. *Journal of Computational Chemistry*, *31*(2), NA-NA. https://doi.org/10.1002/jcc.21334

Weibel, M. K., & Bright, H. J. (1971). The Glucose Oxidase Mechanism: INTERPRETATION OF THE pH DEPENDENCE. *Journal of Biological Chemistry*,

bioRxiv preprint doi: https://doi.org/10.1101/2024.03.20.585966; this version posted March 23, 2024. The copyright holder for this preprint (which was not certified by peer review) is the author/funder. All rights reserved. No reuse allowed without permission.

246(9), 2734–2744. https://doi.org/10.1016/S0021-9258(18)62246-X

Yeom, S. J., Kim, M., Kwon, K. K., Fu, Y., Rha, E., Park, S. H., Lee, H., Kim, H., Lee, D. H., Kim, D. M., & Lee, S. G. (2018). A synthetic microbial biosensor for high-throughput screening of lactam biocatalysts. *Nature Communications 2018 9:1*, *9*(1), 1–12. https://doi.org/10.1038/s41467-018-07488-0

Yoo, E. H., & Lee, S. Y. (2010). Glucose Biosensors: An Overview of Use in Clinical Practice. *Sensors (Basel, Switzerland)*, *10*(5), 4558. https://doi.org/10.3390/S100504558

Zhang, R., & Qian, K. (2023). High-Throughput Screening of Metabolic Biomarkers and Wearable Biosensors for the Quantification of Metabolites. *Advanced Sensor Research*, *2*(3), 2200052. https://doi.org/10.1002/ADSR.202200052